# A dynamic hysteresis model for customized glass transition in amorphous polymer towards multiple shape memory effects

Jingyun Liu[1], Galina Gorbacheva[2], Haibao Lu[1,4], Jiazhi Wang[1,4] and Yong-Qing Fu[3,4]

[1]National Key Laboratory of Science and Technology on Advanced Composites in Special Environments, Harbin Institute of Technology, Harbin 150080, P.R. China

[2]Mytishchi Branch of Federal State Budgetary Educational Institution of Higher Education, Bauman Moscow State Technical University, Mytishchi 141005, Russia

[3]Faculty of Engineering and Environment, Northumbria University, Newcastle upon Tyne NE1 8ST, UK

[4]E-mail: luhb@hit.edu.cn, wangjiazhi@hit.edu.cn and richard.fu@northumbria.ac.uk

**Abstract：** Coexistence of multiple and discrete segments as well as their distinctive hysteresis relaxations enables amorphous shape memory polymers (SMPs) exhibiting complex disordered dynamics, which is critical for the glass transition behavior to determine the shape memory effect (SME), but remained largely unexplored. In this study, a dynamic hysteresis model is proposed to explore the working principle and collective dynamics in discrete segments of amorphous SMPs, towards a dynamic connection between complex relaxation hysteresis and glass transition behavior, which can be applied for design and realization of multiple SMEs in the amorphous SMPs. In combination of free volume theory and Adam-Gibbs domain size model, a phase transition model is formulated to identify the working principle of dynamic relaxation hysteresis in the glass transition of amorphous SMP. Furthermore, constitutive relationships among relaxation time, strain, storage modulus, loss angle

and temperature have been established to describe the dynamic connection between complex relaxation hysteresis and customized glass transition, which is then utilized to achieve multiple SMEs based on the extended Maxwell model. Finally, effectiveness of the proposed models is verified using experimental results of SMPs with multiple SMEs reported in literature.

**Keywords:** shape memory polymer; relaxation hysteresis; glass transition; dynamics

## 1. Introduction

Shape memory polymer (SMP) is one of the distinctive smart materials, which can produce mechanical actuations by regaining their permanent shapes from the deformed ones under external stimuli [1], including heat, light, solvent, electric and magnetic fields [2-6]. Shape memory effect (SME) is originated from the unique thermodynamics of the SMPs whose hard segments maintain their permanent shape, while the soft ones is responsible to trigger reversible shape deformations through their transition behaviors [7]. SMPs have distinctive advantages of large deformation strain, low density and designable properties [8], leading to a variety of practical and potential applications, such as actuation components in microsystem [9], energy storage [10], aerospace deployable structures [11] and biomedical devices [12-14].

Currently, great efforts have been conducted to investigate the working principle of glass transition in dynamic relaxation of the amorphous SMPs. For example, Xie *et al*. [15] shows that Nafion, a polymer with a multi-SME, has shown a wide-range glass transition temperature due to its hysteresis relaxation behavior. Kuang *et al*. [16] reported epoxy SMPs with tunable glass transition behaviors from a single transition

to multiple transitions. Nguyen *et al*. [17] and Yu *et al*. [18] developed multi-branch models to analyze multi-SME in SMP undergoing multiple glass transitions. Nguyen *et al.* [19] developed a viscoelastic model which included three components, viscoelasticity, structural relaxation and stress-activated visco-plasticity in the glassy region. Liu *et al.* [20] proposed a phase-evolution-based constitutive model for amorphous SMPs undergoing reversible transitions between glassy and rubbery phases. Huang *et al.* [21] proposed a constitutive model of amorphous SMPs about their thermomechanical strain rates.

Discrete segments are mentioned in this paper because the soft segments have different relaxation behaviors due to their intrinsic different masses and molecular lengths, which result in a different activation energies and hysteresis of the segments to relax. However, these phenomenological models have not considered relaxation hysteresis and their connections with customized glass transitions into analysis. Currently, no constitutive relationship between relaxation hysteresis and glass transition temperature ($T_g$) has been explored to understand the working principle in multi-SME. It is a great challenge to study the relaxation hysteresis in amorphous SMPs, of which the shape memory behavior is essentially determined by the dynamic glass transition.

In this work, free volume theory [22] and Adams-Gibbs model [23] are employed to identify the phase transitions of amorphous SMPs [24], whose phase transition models have been developed to identify the working principle of complex relaxation hysteresis in a dynamic glass transition. Furthermore, an extend Maxwell model [25]

has been proposed to understand the dynamic connection between relaxation hysteresis and glass transition behavior, which causes the multiple SME in amorphous SMP. Finally, the effectiveness of proposed model is verified using a series of experimental results reported in the literature [16,26-28].

## 2. Theoretical framework

### 2.1 Effect of relaxation hysteresis on glass transition

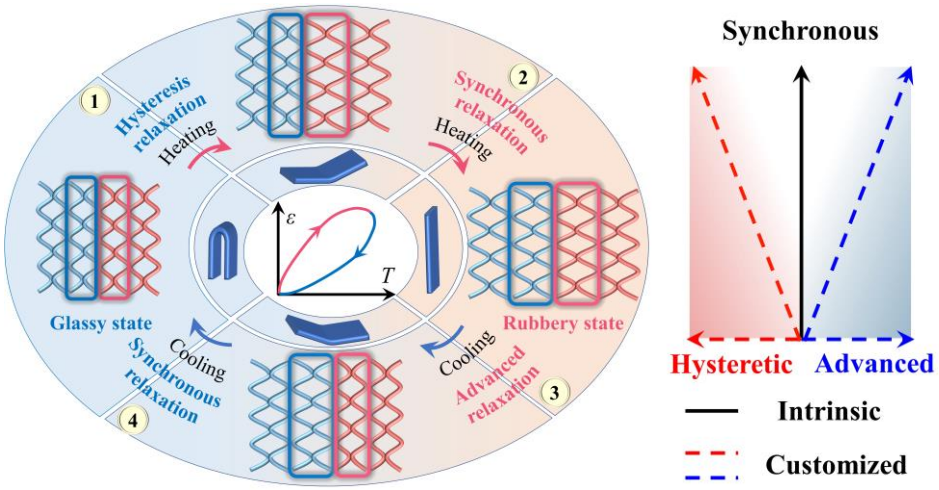


Figure 1. Schematic illustration of the hysteresis, synchronous and advanced relaxations in amorphous SMP, in a heating and cooling cycle.

Figure 1 illustrates the relaxation hysteresis of amorphous SMP. In a heating and cooling cycle, the SMP undergoes glass transition between its glassy state and rubbery state. Meanwhile, the relaxation hysteresis is mainly resulted from the discrete segments, which all have their distinctive dynamic relaxation behaviors in the SMP [29]. With a further increase in temperature, the SMP is in its rubbery state, resulting into a synchronous relaxation of all discrete segments. On the other hand, during the cooling process when the SMP is changed from its rubbery state to glassy state, initially advanced relaxations have been generated in these discrete segments [29]. Then, synchronous relaxations of all discrete segments are generated with a further

decrease in the temperature, because all these discrete segments are in their glassy states. Here the relaxation hysteresis and mechanical energy loss, both which play essential roles in the glass transition behaviors [30], are generated.

Based on the Fox-Flory theory [22], the discrete segments need both activation energy and free volume to relax when the amorphous polymer undergoes a glass transition. The viscosity ($\eta$) can be expressed as [22],

$$\eta=\eta_0 \exp\left(\frac{\gamma V_0}{V_f}+\frac{F_a}{RT}\right) \tag{1}$$

where $\eta_0$ is the initial viscosity of the polymer in its glassy state [22], $\gamma$ is a given constant to characterize the free volume ($0.5\leqslant\gamma\leqslant1$) [31], $V_0$ is the volume occupied by the segments, $V_f$ is the free volume, $F_a$ is the activation energy, $R$=8.314 J/(mol·K) is the molar gas constant and $T$ is the temperature.

For the polymer, the constitutive relationship between free volume ($V_f$) and temperature ($T$) can be written as [22],

$$V_f=\alpha V\left(T-T_0\right) \tag{2}$$

where $\alpha$ is the thermal expansion coefficient of the polymer, $V=V_0+V_f$ is the total volume of polymer and $T_0$ is the temperature at $V_f$=0 [22].

The activation energy of polymer is $F_a=\Delta\mu s^*/S_c$. By substituting equation (2) into equation (1), it can be further rewritten as [23],

$$\eta=\eta_0 \exp\left[\frac{\gamma V_0}{\alpha V\left(T-T_0\right)}+\frac{\Delta\mu s^*}{RTS_c}\right] \tag{3}$$

where $\Delta\mu$ is the average activation energy [32], $s^*$ is the maximum conformational entropy at end-point temperature ($T$*), where all the conformers relax independently [32], and $S_c$ is the conformational entropy at $T$ [32].

The conformational entropy ($S_c$) can be expressed as a function of the temperature ($T$) as [23],

$$S_c = \int_{T_0}^{T} \frac{\Delta C_p}{T} dT \tag{4}$$

where $\Delta C_p$ is the difference in the specific heats of a polymer in glassy and rubbery states.

$\Delta C_p$ varies with $T$ [33],

$$\Delta C_p = \frac{CT_{g0}}{T} \tag{5}$$

where $C$ is a given material constant, $T_{g0}$ is the intrinsic glass transition temperature.

In combination of equations (3), (4) and (5), $\eta$ can be expressed as,

$$\eta = \eta_0 \exp\left[\frac{\gamma V_0}{\alpha V\left(T - T_0\right)} + \frac{\Delta\mu s^* T_0}{RCT_{g0}\left(T - T_0\right)}\right] \tag{6}$$

The relaxation time ($\tau$) is obtained based on the equation (6) [22],

$$\tau = \frac{\eta_0}{E_0} \exp\left[\frac{\gamma V_0}{\alpha V\left(T - T_0\right)} + \frac{\Delta\mu s^* T_0}{RCT_{g0}\left(T - T_0\right)}\right] \tag{7}$$

where $E_0$ is the Young's modulus of amorphous polymer.

To verify the proposed model of equation (7), the relaxation behavior of PLLA-PMMA (PLLA: poly(L-lactide); PMMA: poly(methyl methacrylate)) SMPs was studied using the proposed model. The obtained results are plotted in Figure 2(a), in which the constitutive relationship between relaxation time ($\log\tau$) and temperature ($T$) is varied. All the parameters used in the equation (7) for calculations are listed in

Table 1, with the following given constants, e.g., $\gamma$=0.75 [34], $V_0/V$=0.975 [25,29], $\alpha$=0.048 $K^{-1}$ [25,29], $C$=26.4 J/mol·K [33,35], $T_{g0}/T_0$ =1.26 [23] and $\Delta\mu s^*/R$=16.13 kJ/mol·K [23]. Results in Figure 2(a) show that the end-point temperature ($T^*$) of PLLA-PMMA SMP is increased from 356 K, 367 K to 373 K at the same relaxation time of $\tau=10^{-4.83}$ s, with an increase of volume content of PMMA from 0, 30% to 50%. Figure 2(b) shows the divergence of the analytical results and experimental data calculated based on the correlation index ($R^2$), of which the values are 97.98%, 98.49% and 98.99%, when the volume content of PMMA is increased from 0%, 30% to 50%. The analytical and experimental results reveal that the end-point temperature ($T^*$) of PLLA-PMMA SMPs has been increased with the increase in volume content of PMMA, which works as a hard segment and has a higher glass transition temperature than that of the PLLA.

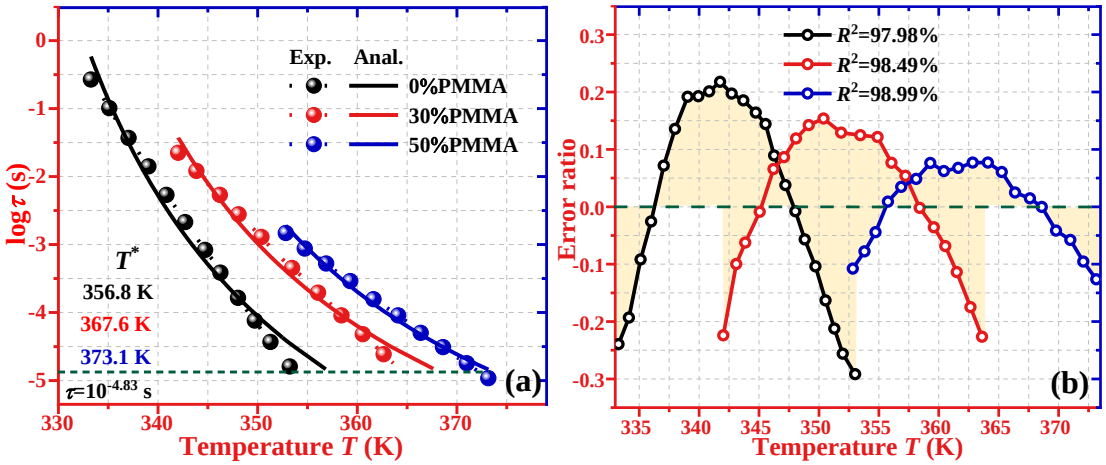


Figure 2. Analytical results of equation (7) and experimental data [26] of relaxation time (log$\tau$) for the PLLA-PMMA SMPs with various volume contents of PMMA. (a) For the relaxation time-temperature curves. (b) Divergences of the analytical and experimental results.

Table 1. Values of parameters used in equation (7) for PLLA-PMMA SMPs with various volume contents of PMMA [26].

| PMMA (%) | $\eta_0/E_0$ (s) | $T_0$ (K) |
|---|---|---|
| 0 | $10^{-9.44}$ | 309.68 |
| 30 | $10^{-8.76}$ | 312.42 |
| 50 | $10^{-8.65}$ | 316.20 |

According to the phase transition theory [24], the phase evolution function ($\phi_f$) of SMP is determined by the stored strain ($\varepsilon_s$) and pre-stored strain ($\varepsilon_{pre}$) with the expression as follows,

$$\phi_f = \frac{\varepsilon_s}{\varepsilon_{pre}} = 1 - A\exp\left[-\frac{\gamma V_0}{\alpha V\left(T-T_0\right)} - \frac{\Delta\mu s^* T_0}{RCT_{g0}\left(T-T_0\right)}\right] \quad (8)$$

where $A$ is a material constant.

In combination of equation (8) and $\varepsilon_s=\varepsilon-\varepsilon_0$ ($\varepsilon$ is the total strain, $\varepsilon_0$ is the initial strain and $\varepsilon_s$ is the stored strain), the total strain ($\varepsilon$) can be expressed as,

$$\varepsilon=\varepsilon_0+\varepsilon_s = \varepsilon_0 + \varepsilon_{pre}\phi_f = \varepsilon_0 + \varepsilon_{pre}\left\{1 - A\exp\left[-\frac{\gamma V_0}{\alpha V\left(T-T_0\right)} - \frac{\Delta\mu s^* T_0}{RCT_{g0}\left(T-T_0\right)}\right]\right\} \quad (9)$$

To verify the equation (9), analytical results of strain ($\varepsilon$) as a function of temperature ($T$) for amorphous SMP have been obtained and the results are plotted in Figure 3(a). The following parameters are used $A$=71.88, $\gamma$=0.75 [34], $V_0/V$=0.975 [25,29], $\alpha$=0.048/K [25,29], $C$=26.4 J/mol·K [33,35], $T_{g0}/T_0$ =1.26 [23], $\varepsilon_0$=0, $\varepsilon_{pre}$=6% and $\Delta\mu s^*/R$=8 kJ/mol·K. The maximum slope of the strain curve shown in Figure 3(a) is defined as the glass transition temperature ($T_g$) [22]. With an increase in $T_0$ from 320 K, 330 K, 340 K, 350 K to 360 K, the glass transition temperature ($T_g$) is gradually increased from 372 K, 382 K, 392 K, 402 K to 412 K. Figure 3(b) shows the analytical results of strains as a function of temperature, plotted at different values

of $\Delta\mu s^*/R$=4 kJ/mol·K, 5 kJ/mol·K, 6 kJ/mol·K, 7 kJ/mol·K and 8 kJ/mol·K, in order to identify the effect of activation energy on the glass transition temperature ($T_g$) of SMP. The glass transition temperature ($T_g$) is increased from 367 K, 373 K, 379 K, 385 K to 392 K with an increase in the $\Delta\mu s^*/R$ from 4 kJ/mol·K, 5 kJ/mol·K, 6 kJ/mol·K, 7 kJ/mol·K to 8 kJ/mol·K, at $T_0$=340 K. With the increment of activation energy ($\Delta\mu s^*/R$), the segment needs more energy to relax, causing a higher $T_g$.

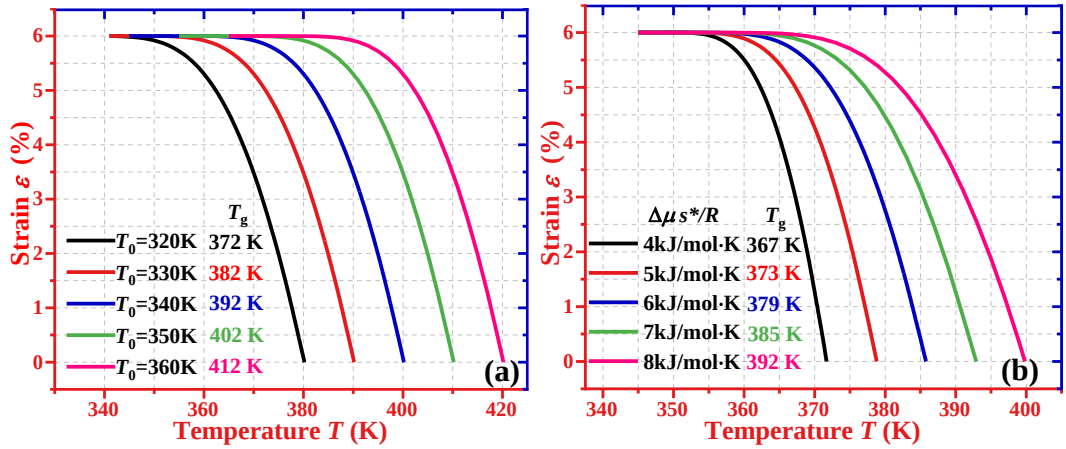


Figure 3. (a) Analytical results of equation (9) for the strain as a function of temperature at a given value of $T_0$=320 K, 330 K, 340 K, 350 K and 360 K, when $\Delta\mu s^*/R$=8 kJ/mol·K. (b) Analytical results of equation (9) for the strain as a function of temperature at a given value of $\Delta\mu s^*/R$=4 kJ/mol·K, 5 kJ/mol·K, 6 kJ/mol·K, 7 kJ/mol·K and 8 kJ/mol·K, when $T_0$=340 K.

Furthermore, the analytical results based on the equation (9) are plotted in Figure 4, together with the experimental data [27] of DETDA-D230 (DETDA: Diethyltoluenediamine; D230: poly(propylene glycol) bis (2-aminopropyl) ether) SMP with various molar ratios of DETDA of 0, 60% and 100%, at given values of parameters of $A$=71.88, $\gamma$=0.75 [34], $V_0/V$=0.975 [25,29], $\alpha$=0.048 $K^{-1}$ [25,29], $C$=26.4 J/mol·K [33,35] and $T_{g0}/T_0$ =1.26 [23]. The parameters listed in Table 2 were used to predict the strain as a function of temperature, and the analytical and experimental results of strains as a function of temperature are plotted in Figure 4(a). It is found

that the analytical results are in good agreements with the experimental ones. With an increase in the molar ratio of DETDA from 0%, 60% to 100%, the DETDA-D230 SMPs complete their strain recoveries at 366.5 K, 397.5 K and 422.5 K, respectively, when $\varepsilon$=0.55%. The analytical results can be well explained, e.g., the glass transition temperature ($T_g$) of SMP is increased with the increase in molar ratio of hard segment, of which the $T_g$ is higher than that of the soft segments. Furthermore, the divergences between the analytical and experimental results [27] of the DETDA-D230 SMPs were calculated using the correlation index ($R^2$), and the obtained results are 92.00%, 94.56% and 96.68% for the SMPs with various molar ratios of DETDA of 0%, 60% and 100%, as shown in Figure 4(b).

Table 2. Values of parameters used in equation (9) for DETDA-D230 SMPs [27].

| DETDA (%) | $\Delta\mu s^*/R$ (kJ/mol·K) | $T_0$ (K) |
|---|---|---|
| 0 | 3.53 | 337.97 |
| 60 | 5.88 | 352.24 |
| 100 | 8.04 | 361.34 |

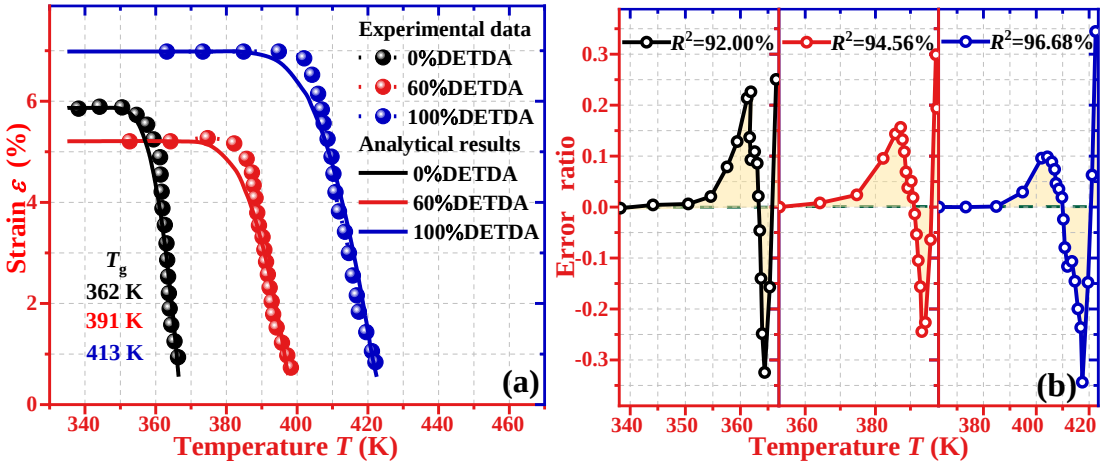


Figure 4. Comparisons between the analytical results of equation (9) and the experimental data [27] of the DETDA-D230 SMPs with various molar ratio of DETDA of 0, 60% and 100%. (a) For the strain-temperature curves. (b) Divergences of the analytical and experimental results.

## 2.2 Dynamic connection between relaxation hysteresis and glass transition

Dynamic behavior of SMP has been critically determined by the relaxation hysteresis of soft segments, which present a variety of glass transition temperatures ($T_g$). Figure 5(a) illustrates the extended Maxwell model with three dynamic components, i.e., an equilibrium branch, a non-equilibrium branch and a hysteresis branch, in a parallel manner. Furthermore, there are other three dynamic components in the hysteresis branch, i.e., a hysteretic sub-branch, a synchronous sub-branch and an advanced sub-branch. The proposed model is then used to characterize the dynamic relaxation for the SMP, which show a hysteretic relaxation behavior in the heating process, while it shows an advanced relaxation behavior in the cooling process. Here, the dynamic relaxation behavior is determined by the loss angel ($\delta$), which causes a higher modulus in the heating process and a lower modulus in the cooling process, as shown in Figure 5(b).

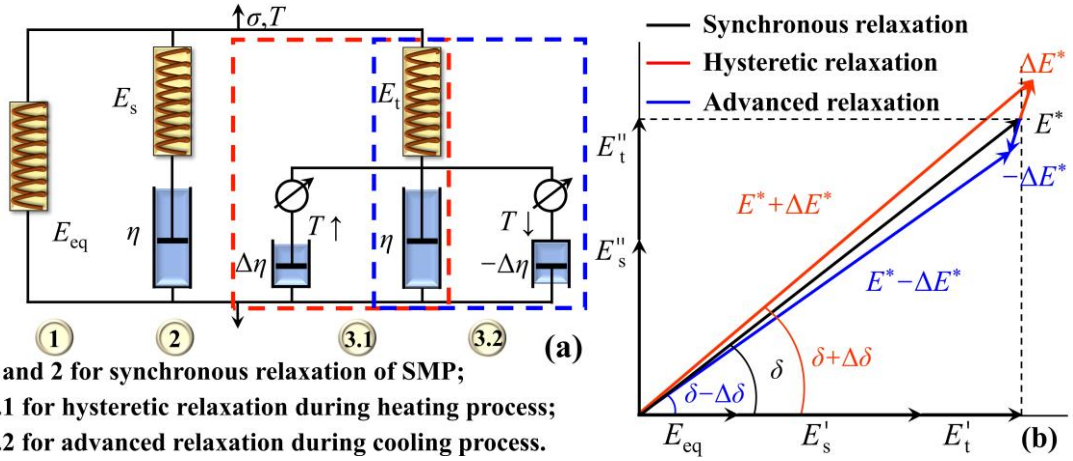


Figure 5. (a) Schematic illustrations of three dynamic branches to describe the relaxation behavior of amorphous SMP in terms of the extend-Maxwell model. (b) Modulus parameter as a function of loss angel ($\delta$) for the hysteretic, synchronous and advanced relaxations in amorphous SMP.

Based on the extended Maxwell model, the stress and strain can be expressed as follows [25],

$$\sigma = \sigma_{eq} + \sigma_s + \sigma_t, \quad \varepsilon = \varepsilon_{eq} = \varepsilon_s = \varepsilon_t \tag{10}$$

where $\sigma$ and $\varepsilon$ are the stress and strain of the SMP; $\sigma_{eq}$ and $\varepsilon_{eq}$ are the stress and strain of the equilibrium branch; $\sigma_s$ and $\varepsilon_s$ are the stress and strain of the non-equilibrium branch; and $\sigma_t$ and $\varepsilon_t$ are the stress and strain of hysteresis branch, respectively.

Then, the viscoelastic constitutive stress-strain relationship can be obtained as [25],

$$\varepsilon = \frac{\sigma_{eq}}{E_{eq}} \tag{11a}$$

$$\frac{d\varepsilon}{dt} = \frac{1}{E_s}\frac{d\sigma_s}{dt} + \frac{\sigma_s}{\eta} \tag{11b}$$

$$\frac{d\varepsilon}{dt} = \frac{1}{E_t}\frac{d\sigma_t}{dt} + \frac{\sigma_t}{\eta \pm \Delta\eta} \tag{11c}$$

where $E_{eq}$, $E_s$ and $E_t$ are the moduli of the equilibrium, non-equilibrium and hysteresis branches, respectively, $\eta$ is the viscosity of the synchronous relaxation component, $\pm\Delta\eta$ is the hysteretic and advanced relaxation components, respectively.

Substituting equation (11) into (10), the stress ($\sigma$) can be obtained as,

$$\begin{aligned}\sigma(t) &= \sigma_{eq} + \sigma_s + \sigma_t \\ &= \left( E_{eq} + \frac{\omega^2\tau_s^2 + i\omega\tau_s}{1+\omega^2\tau_s^2}E_s + \frac{\omega^2\tau_t^2 + i\omega\tau_t}{1+\omega^2\tau_t^2}E_t \right) \cdot \varepsilon_0 \exp(i\omega t)\end{aligned} \tag{12}$$

where $\tau_s$ and $\tau_t$ are the relaxation times of the synchronous relaxation and hysteretic relaxation, respectively, and $\varepsilon(t)=\varepsilon_0\exp(i\omega t)$ ($i=\sqrt{-1}$, $\omega$ is the angle frequency).

Then, the modulus ($E^*$) can be obtained as,

$$E^* = \frac{\sigma(t)}{\varepsilon(t)} = E_{eq} + E_s\frac{\omega^2\tau_s^2}{1+\omega^2\tau_s^2} + E_t\frac{\omega^2\tau_t^2}{1+\omega^2\tau_t^2} + E_s\frac{i\omega\tau_s}{1+\omega^2\tau_s^2} + E_t\frac{i\omega\tau_t}{1+\omega^2\tau_t^2} \tag{13}$$

Furthermore, the $\tau_s$ and $\tau_t$ can also be obtained as,

$$\tau_s = \frac{\eta}{E_s} \tag{14a}$$

$$\tau_t = \frac{\eta \pm \Delta\eta}{E_t} \tag{14b}$$

In combination of equations (13) and (14), the storage modulus and loss modulus can be expressed as [25,29],

$$E' = E_{eq} + E_s \frac{\omega^2\tau_s^2}{1+\omega^2\tau_s^2} + E_t \frac{\omega^2\tau_t^2}{1+\omega^2\tau_t^2} \tag{15a}$$

$$E'' = E_s \frac{\omega\tau_s}{1+\omega^2\tau_s^2} + E_t \frac{\omega\tau_t}{1+\omega^2\tau_t^2} \tag{15b}$$

The loss angle (tan$\delta$) of SMP is obtained [25],

$$\tan\delta = \frac{E''}{E'} \tag{16}$$

Finally, the constitutive stress-strain relationship of the SMP has been obtained,

$$\sigma = \sigma_{eq} + \sigma_s + \sigma_t = E_{eq}\varepsilon + \dot{\varepsilon}\tau_s E_s\left[1-\exp\left(-\frac{\varepsilon/\dot{\varepsilon}}{\tau_s}\right)\right] + \dot{\varepsilon}\tau_t E_t\left[1-\exp\left(-\frac{\varepsilon/\dot{\varepsilon}}{\tau_t}\right)\right] \tag{17}$$

where $\varepsilon=\dot{\varepsilon}t$ (where $\dot{\varepsilon}$ is the strain rate).

To identify the working principles for synchronous and hysteretic relaxations, the effect of temperature on the storage modulus of SMP has been investigated based on equation (15), and the obtained results are shown in Figure 6. The parameters used in equation (15) are $E_{eq}$=10 MPa, $E_s$=6200 MPa, $E_t$=150 MPa [16], $\omega$=0.01 $s^{-1}$ [25], $\eta$=23.7 MPa·s [36,37], $\gamma$=0.75 [34], $V_0/V$=0.975 [25,29], $\alpha$=0.048 $K^{-1}$ [25,29], $C$=26.4 J/mol·K [33,35], $T_{g0}/T_0$=1.26 [23], $\Delta\mu s^*/R$=9.76 kJ/mol·K [23] and $T_0$=295 K. The analytical results of storage moduli as a function of temperature are plotted in Figure 6(a). When the differences in viscosity values ($\Delta\eta$) of synchronous and hysteretic branches are increased from 0 MPa·s, 25 MPa·s, 50 MPa·s, 75 MPa·s to 100 MPa·s, the glass transition temperature ($T_{g2}$) is gradually increased from 343 K, 349 K, 353

K, 356 K to 359 K, at the same storage modulus of $E'$=85 MPa. It reveals that the glass transition temperature ($T_{g2}$) is increased with the increment of the difference in viscosity of synchronous and hysteretic branches. Effects of the advanced relaxation on the storage modulus were investigated for the SMPs, which undergo two glass transitions, i.e., $T_{g1}$=325 K and $T_{g2}$, and the obtained results are shown in Figure 6(b). At the same storage modulus of 85 MPa, the glass transition temperature ($T_{g2}$) is gradually decreased from 343 K, 342 K, 340 K, 338 K to 336 K with a decrease in the difference in viscosity ($\Delta\eta$) of synchronous and advanced branches from 0 MPa·s, -5 MPa·s, -10 MPa·s, -15 MPa·s to -20 MPa·s. These analytical results reveal that a larger difference in viscosity ($\Delta\eta$) of synchronous and advanced branches, a lower glass transition temperature ($T_{g2}$) of the SMP is observed.

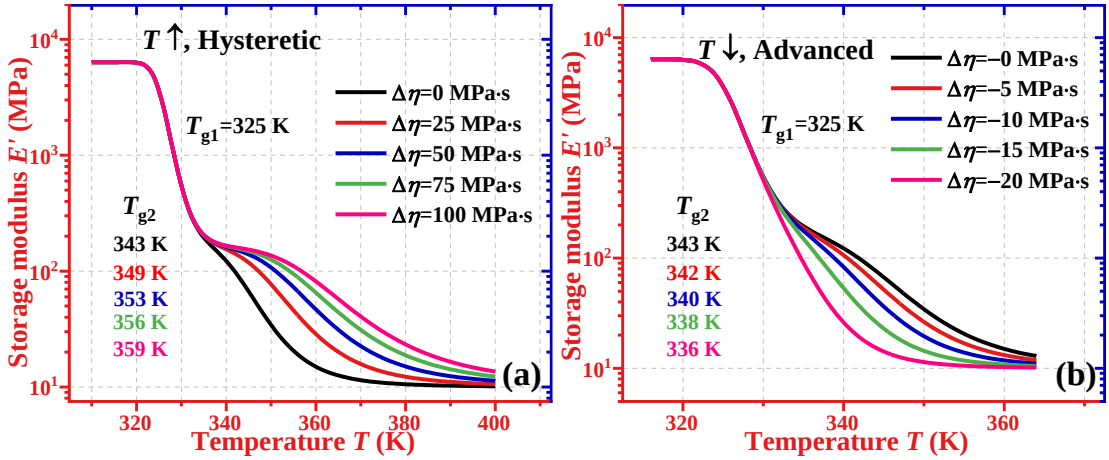


Figure 6. Constitutive storage modulus-temperature relationships. (a) Analytical results of SMP in heating process, with the difference in viscosity ($\Delta\eta$) of synchronous and hysteretic relaxations increased from 0 MPa·s, 25 MPa·s, 50 MPa·s, 75 MPa·s and 100 MPa·s. (b) Analytical results of SMP in cooling process, with the difference in viscosity ($\Delta\eta$) of synchronous and advanced relaxations decreased from 0 MPa·s, -5 MPa·s, -10 MPa·s, -15 MPa·s and -20 MPa·s.

The analytical results of loss angles (tan$\delta$) as a function of temperature were further studied to investigate the effect of relaxation hysteresis on the glass transition

temperature ($T_g$) of the SMP, and the obtained results are shown in Figure 7. The parameters used in the calculations using the equations (15) and (16) are $E_{eq}$=10 MPa, $E_s$=6200 MPa, $E_t$=150 MPa [16], $\omega$=0.01 $s^{-1}$ [25], $\eta$=23.7 MPa·s [36,37], $\gamma$=0.75 [34], $V_0/V$=0.975 [25,29], $\alpha$=0.048 $K^{-1}$ [25,29], $C$=26.4 J/mol·K [33,35], $T_{g0}/T_0$=1.26 [23], $\Delta\mu s^*/R$=9.76 kJ/mol·K [23] and $T_0$=295 K. Figure 7(a) shows the analytical results of loss angle (tan$\delta$) of SMPs, of which dual SME is achieved by $T_{g1}$=332 K and $T_{g2}$, with various differences in viscosity of synchronous and hysteretic relaxations, e.g., $\Delta\eta$=0 MPa·s, 25 MPa·s, 50 MPa·s, 75 MPa·s and 100 MPa·s, and the glass transition temperatures ($T_{g2}$) are 339 K, 346 K, 348 K, 351 K and 354 K during the heating process. It is revealed that the glass transition temperature ($T_{g2}$) is gradually increased with an increase in the difference in viscosity of synchronous and hysteretic relaxations. Effects of differences in viscosity of synchronous and advanced branches on the loss angle (tan$\delta$) have been investigated, and the obtained results are shown in Figure 7(b). The parameters used in equations (15) and (16) are $E_{eq}$=135 MPa, $E_s$=150 MPa, $E_t$=978 MPa [28], $\omega$=0.01 $s^{-1}$ [25,29], $\eta$=5.21 MPa·s [36,37], $\gamma$=0.75 [34], $V_0/V$=0.975 [25,29], $\alpha$=0.048 $K^{-1}$ [25,29], $C$=26.4 J/mol·K [33,35], $T_{g0}/T_0$=1.26 [23], $\Delta\mu s^*/R$= 10.42 kJ/mol·K [23] and $T_0$=278 K. The glass transition temperature ($T_{g1}$) of SMPs, of which dual SME is achieved by $T_{g1}$ and $T_{g2}$=320 K, is decreased from 316 K, 314 K, 312 K, 311 K to 309 K during the cooling process with a decrease in the difference in viscosity ($\Delta\eta$) of synchronous and advanced branches from 0 MPa·s, -1 MPa·s, -2 MPa·s, -3 MPa·s to -4 MPa·s. These analytical results reveal that the glass

transition temperature ($T_{g1}$) is gradually decreased with an increase in the differences in viscosity of synchronous and advanced relaxations.

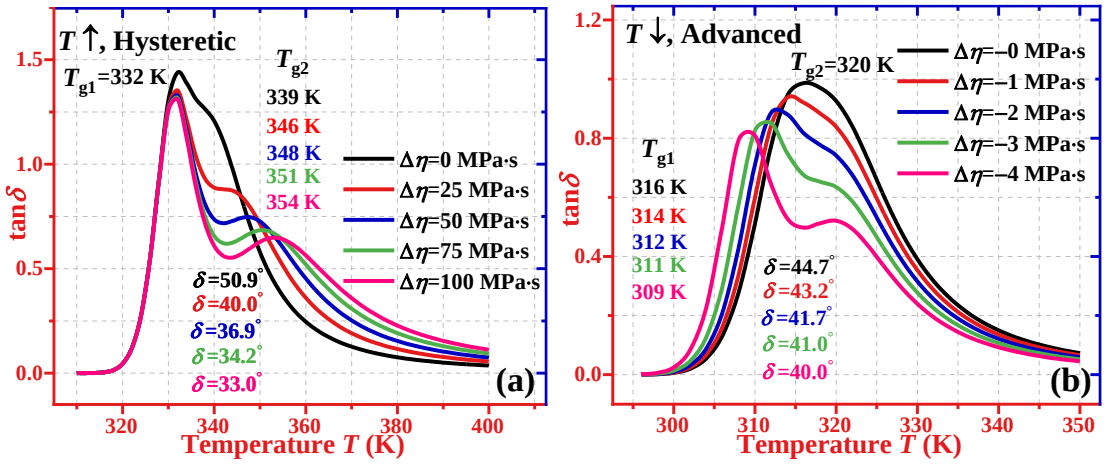


Figure 7. Effects of hysteretic and advanced relaxations on the loss angle (tan$\delta$). (a) Analytical results of equation (16) for the loss angle (tan$\delta$) as a function of temperature at a given value of $\Delta\eta$=0 MPa·s, 25 MPa·s, 50 MPa·s, 75 MPa·s, and 100 MPa·s. (b) Analytical results of equation (16) for the loss angle (tan$\delta$) as a function of temperature at a given value of $\Delta\eta$=0 MPa·s, -1 MPa·s, -2 MPa·s, -3 MPa·s, and -4 MPa·s.

To further identify the working principle of relaxation hysteresis in the amorphous SMP, the constitutive stress-strain relationship has been investigated based on equation (17), and the results are shown in Figure 8. The parameters used in equation (17) are $E_{eq}$=10 MPa, $E_s$=978 MPa, $E_t$=250 MPa [28] and $\eta$=5.21 MPa·s [36,37]. Figure 8(a) shows that the stress ($\sigma$) is increased from 5.48 MPa, 12.96 MPa, 20.00 MPa, 25.88 MPa to 30.57 MPa, at given strain of $\varepsilon$=23.5% and strain rate of $\dot{\varepsilon}$=0.3 $s^{-1}$, for the SMP in the heating process, where the difference in viscosity ($\Delta\eta$) of synchronous and hysteretic relaxations is increased from 0 MPa·s, 25 MPa·s, 50 MPa·s, 75 MPa·s to 100 MPa·s. Figure 8(b) shows that the stress is gradually decreased from 34.88 MPa, 32.18 MPa, 29.31 MPa, 26.35 MPa to 23.35 MPa at a given strain ($\varepsilon$) of 23.5% and strain rate of $\dot{\varepsilon}$=0.3 $s^{-1}$, with the difference in viscosity

($\Delta\eta$) of synchronous and advanced relaxations decreased from 0 MPa·s, -10 MPa·s, -20 MPa·s, -30 MPa·s to -40 MPa·s.

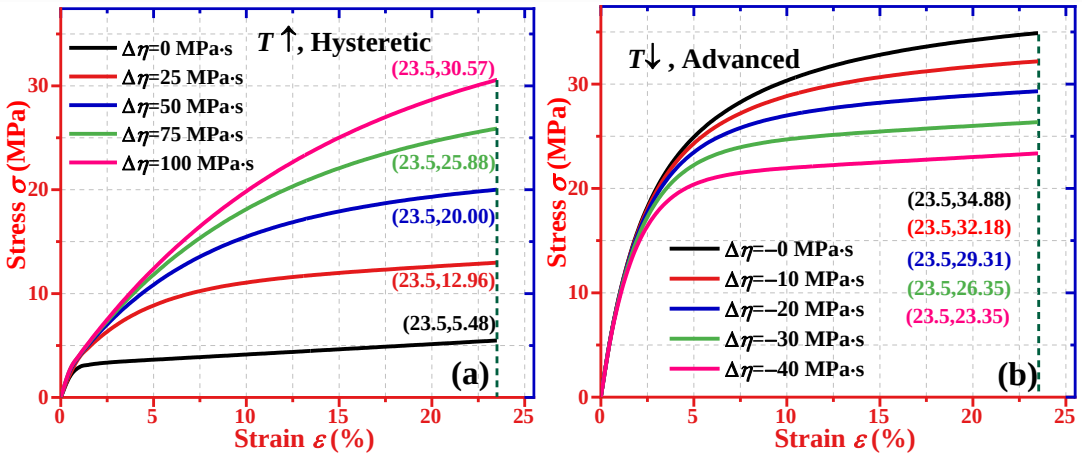


Figure 8. Constitutive stress-strain relationship curves of SMPs. (a) For the constitutive stress-strain relationship curves of SMPs undergoing hysteresis relaxation, with a given difference in viscosity ($\Delta\eta$) of 0 MPa·s, 25 MPa·s, 50 MPa·s, 75 MPa·s and 100 MPa·s. (b) For the constitutive stress-strain relationship curves of SMPs undergoing advanced relaxation, with a given difference in viscosity ($\Delta\eta$) of 0 MPa·s, -10 MPa·s, -20 MPa·s, -30 MPa·s, and -40 MPa·s.

## 3. Experimental verification

Experimental data [16] of DGEBA (Diglycidyl ether bisphenol A) SMP with molar contents of diamine Diels–Alder adduct (FM) cross-linker of 33%, 67% and 100%, have been employed to verify the analytical results generated from the proposed models of equations (15) and (16). All the parameters used in the calculation using the equations (15) and (16) are $\omega$=0.01 $s^{-1}$ [25], $\gamma$=0.75 [34], $V_0/V$=0.975 [25,29], $\alpha$=0.048 $K^{-1}$ [25,29], $C$=26.4 J/mol·K [33,35] and $T_{g0}/T_0$ =1.26 [23].

With an increase in the molar content of FM from 33%, 67% to 100%, the glass transition temperature ($T_g$) of DGEBA SMP is gradually decreased from 350.2 K, 344.3 K to 336.1 K, and simultaneously the storage modulus is increased from 29.48 MPa, 35.57 MPa to 186.48 MPa. As shown in Figures 9(a), (c) and (e), the loss angle

(tan$\delta$) is also increased from 51.6°, 52.9° to 53.5° with an increase in the molar content of FM from 33%, 67% to 100%. These experimental and analytical results reveal that more segments have been involved to improve the mechanical properties of DGEBA SMP, thus resulting in an increased storage modulus with an increase in the molar FM content. On the other hand, the loss angle (tan$\delta$) is also increased because the loss modulus is improved due to the increase in viscosity. This can cause the decrease in the glass transition temperature ($T_g$). Therefore, with an increase in the molar FM content, both the storage modulus and loss angle (tan$\delta$) are increased, while the $T_g$ is decreased. In Figures 9(b), (d) and (f), the divergences between the analytical and experimental results of the storage modulus were analyzed by calculating the correlation index ($R^2$), which are 97.29%, 98.03% and 97.25% at molar content of FM of 33%, 67% and 100%, respectively. Meanwhile, the correlation indexs ($R^2$) are 96.74%, 95.85% and 94.64% for the loss angle (tan$\delta$).

Table 3. Values of parameters used in equations (15) and (16) for DGEBA SMPs [16].

| FM (%) | $E_{eq}$ (MPa) | $E_s$ (MPa) | $E_t$ (MPa) | $\Delta\mu s^*/R$ (kJ/mol·K) | $\eta$ (MPa·s) | $\Delta\eta$ (MPa·s) | $T_0$ (K) |
|---|---|---|---|---|---|---|---|
| 33 | 200 | 2400 | 384 | 7.74 | 10 | 0.01 | 319.5 |
| 67 | 190.9 | 3000 | 500 | 8.03 | 17.73 | 4.43 | 308 |
| 100 | 300 | 6200 | 498 | 10.44 | 23.7 | 34.39 | 300 |

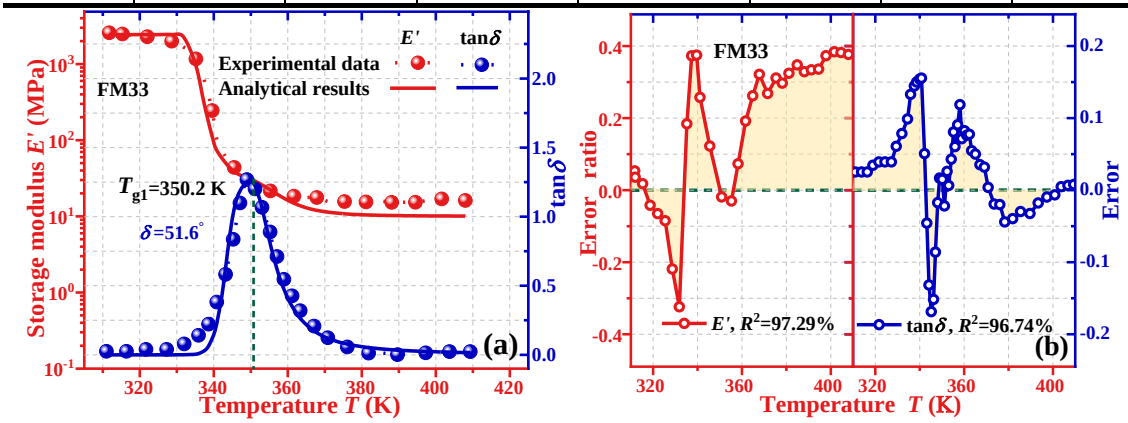

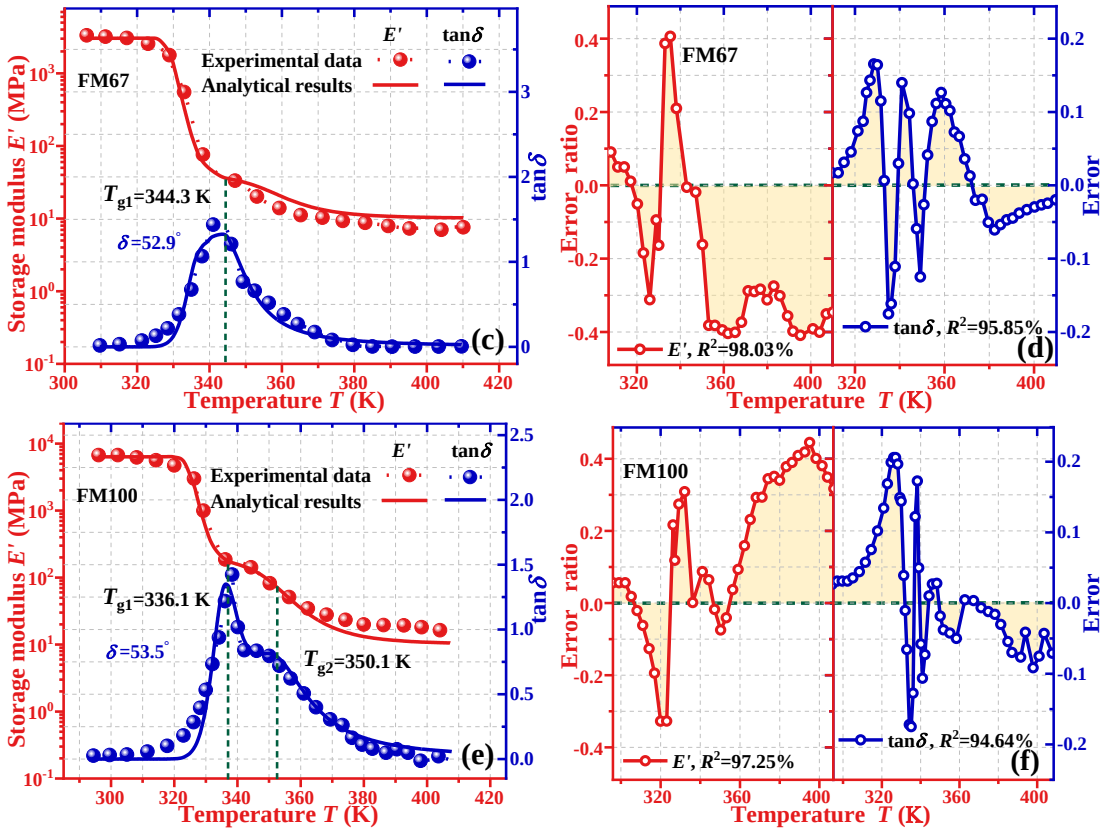


Figure 9. Comparisons of analytical and experimental results [16] for the storage modulus and loss angle (tan$\delta$) as a function of temperature of DGEBA SMPs with various molar contents of FM cross-linker of 33%, 67% and 100%. (a), (c) and (e) For the storage modulus-temperature and loss angle (tan$\delta$)-temperature curves. (b), (d) and (f) Divergences of the analytical and experimental results of DGEBA SMPs with molar contents of FM of 33%, 67% and 100%, respectively.

Furthermore, effect of cooling rate on the loss angle (tan$\delta$) has also been investigated to identify the working principle of dynamic relaxation hysteresis in the SMP. The obtained analytical results of loss angle (tan$\delta$) as a function of temperature are shown in Figure 10(a), which also includes the experimental data of epoxy SMP reported in Ref. [28]. The parameters used in equation (16) are listed in Table 4, where $E_{eq}$=135 MPa, $E_s$=150 MPa and $E_t$=978 MPa [28]. These experimental and analytical results reveal that the $T_g$ is gradually decreased from 316.4 K, 308.0 K to 307.3 K, with the cooling rate increased from 3 K/min, 5 K/min to 7 K/min.

Meanwhile, the loss angle ($\delta$) is decreased from 44.7°, 42.3° to 41.3°. The analytical results obtained using the proposed models are in good agreements with the experimental data of epoxy SMP reported in Ref. [28], which undergo advanced relaxation processes with a variety of cooling rates. The divergences between the analytical and experimental results [28] of the epoxy SMP were analyzed using the correlation index ($R^2$), which are 96.33%, 94.70% and 93.44% for epoxy SMP, at a cooling rate of 3 K/min, 5 K/min and 7 K/min, respectively, as shown in Figure 10(b).

Table 4. Values of parameters used in equation (16) for epoxy SMPs [28].

| Cooling rate (K/min) | $\Delta\mu s^*/R$ (kJ/mol·K) | $\eta$ (MPa·s) | $\Delta\eta$ (MPa·s) | $T_0$ (K) |
|---|---|---|---|---|
| 3 | 10.42 | 5.21 | -0.01 | 277.8 |
| 5 | 10.96 | 7.83 | -2.63 | 268.1 |
| 7 | 11.64 | 9.73 | -4.53 | 264.0 |

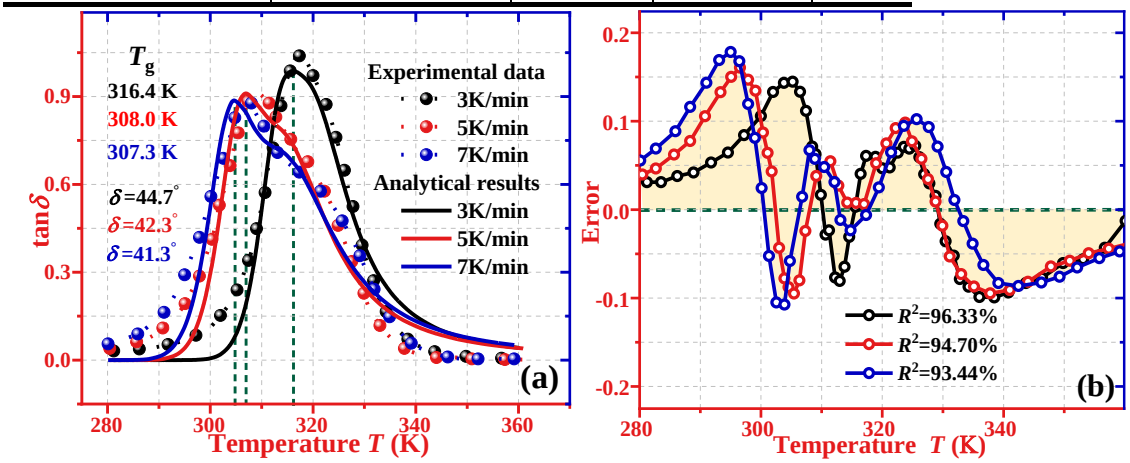


Figure 10. Comparisons of analytical and experimental results [28] for the loss angle (tan$\delta$) as a function of temperature of epoxy SMP undergoing various cooling rates of 3 K/min, 5 K/min and 7 K/min. (a) For the loss angle (tan$\delta$)-temperature curves. (b) Divergences of the analytical and experimental results.

## 4. Conclusion

In this study, we develop a hysteresis model to explore the dynamic connection between complex relaxation hysteresis and glass transition behavior in the amorphous

SMPs, to achieve a customized and multiple SME. Coexistence of multiple and discrete segments as well as their dynamic hysteresis relaxations enables the amorphous SMP exhibit a complex disorder of collective dynamics, which has been well modeled in the present study, based on the free volume theory and Adam-Gibbs model. A phase transition model is then formulated to identify the complex disorder and collective dynamics of relaxation hysteresis in dynamic glass transition. Furthermore, a dynamic connection between complex relaxation hysteresis and customized glass transition, which cause the generation of multiple SMEs, has been proposed to explore the effects of temperature, heating/cooling rate and viscosity on the thermomechanical and shape memory behaviors. Finally, the accuracy of analytical results of proposed models has been verified using the experimental data reported in literature. This study is expected to provide a new strategy for multiple SME in SMPs, based on the complex relaxation hysteresis towards customized glass transition.

**Acknowledgements**

This work was financially supported by the National Natural Science Foundation of China (NSFC) under Grant No. 11725208 and 12172107, International Exchange Grant (IEC/NSFC/201078) through Royal Society and NFSC.

**Appendix A.**

The viscoelastic constitutive stress-strain relationship of the extend Maxwell model can be obtained as [25],

$$\varepsilon = \frac{\sigma_{\mathrm{eq}}}{E_{\mathrm{eq}}} \tag{A1a}$$

$$\frac{\mathrm{d}\varepsilon}{\mathrm{d}t} = \frac{1}{E_{\mathrm{s}}}\frac{\mathrm{d}\sigma_{\mathrm{s}}}{\mathrm{d}t} + \frac{\sigma_{\mathrm{s}}}{\eta} \tag{A1b}$$

$$\frac{\mathrm{d}\varepsilon}{\mathrm{d}t} = \frac{1}{E_{\mathrm{t}}}\frac{\mathrm{d}\sigma_{\mathrm{t}}}{\mathrm{d}t} + \frac{\sigma_{\mathrm{t}}}{\eta \pm \Delta\eta} \tag{A1c}$$

where $E_{\mathrm{eq}}$, $E_{\mathrm{s}}$ and $E_{\mathrm{t}}$ are the moduli of the equilibrium, non-equilibrium and hysteresis branches, respectively, $\eta$ is the viscosity of the synchronous relaxation component, $\pm\Delta\eta$ is the hysteretic and advanced relaxation components, respectively.

When the SMP is loaded under a uniaxial tensile strain of $\varepsilon=\dot{\varepsilon}t$ (where $\dot{\varepsilon}$ is the strain rate [28]), the stresses $\sigma_{\mathrm{eq}}$ of equilibrium branches can be expressed as,

$$\sigma_{\mathrm{eq}} = E_{\mathrm{eq}}\varepsilon \tag{A2}$$

Assuming that $\sigma_{\mathrm{s}}=A\exp(Bt)+C$, then we can obtain $\sigma_{\mathrm{s}}=A+C=0$ at $t=0$,

$$\sigma_{\mathrm{s}} = C\left[1-\exp\left(Bt\right)\right] \tag{A3}$$

Substituting equation (A3) into (A1b), equation (A1b) can be re-written as

$$\dot{\varepsilon} = \left(\frac{B}{E_{\mathrm{s}}} + \frac{1}{\eta}\right)\left[-C\exp\left(Bt\right)\right] + \frac{C}{\eta} \tag{A4}$$

In equation (A4), the following conditions need to be satisfied,

$$C = \dot{\varepsilon}\eta,\ B = -\frac{E_{\mathrm{s}}}{\eta} \tag{A5}$$

Combining equations (A3) and (A5), the stress $\sigma_{\mathrm{s}}$ of non-equilibrium branch can be expressed as,

$$\sigma_s = \dot{\varepsilon}\tau_s E_s\left[1-\exp\left(-\frac{\varepsilon/\dot{\varepsilon}}{\tau_s}\right)\right],(\tau_s = \frac{\eta}{E_s}) \tag{A6}$$

Similarly, the stress $\sigma_s$, the stress $\sigma_t$ in the non-equilibrium branch can be derived as,

$$\sigma_t = \dot{\varepsilon}\tau_t E_t\left[1-\exp\left(-\frac{\varepsilon/\dot{\varepsilon}}{\tau_t}\right)\right],(\tau_t = \frac{\eta}{E_t}) \tag{A7}$$

Finally, the constitutive stress-strain relationship of the SMP can be obtained by combining equations (A2), (A6) and (A7),

$$\sigma(\varepsilon) = \sigma_{eq} + \sigma_s + \sigma_t = E_{eq}\varepsilon + \dot{\varepsilon}\tau_s E_s\left[1-\exp\left(-\frac{\varepsilon/\dot{\varepsilon}}{\tau_s}\right)\right] + \dot{\varepsilon}\tau_t E_t\left[1-\exp\left(-\frac{\varepsilon/\dot{\varepsilon}}{\tau_t}\right)\right] \tag{A8}$$

**References**


[1] Fang Y, Ni Y L, Leo S Y, Taylor C, Basile V and Jiang P 2015 Reconfigurable photonic crystals enabled by pressure-responsive shape-memory polymers *Nat. Commun.* **6** 1–8

[2] Lu H B, Liu Y J, Leng J S and Du S Y 2009 Qualitative separation of the effect of the solubility parameter on the recovery behavior of shape-memory polymer *Smart Mater. Struct.* **18** 085003

[3] Yang B, Huang W M, Li C, Lee C M and Li L 2004 On the effects of moisture in a polyurethane shape memory polymer *Smart Mater. Struct.* **3** 191–5

[4] Lu H B, Liu Y J, Leng J S and Du S Y 2010 Qualitative separation of the physical swelling effect on the recovery behavior of shape memory polymer *Eur. Polym. J.* **46** 1908–14

[5] Ji S B, Fan F Q, Sun C X, Yu Y and Xu H P 2017 Visible light-induced plasticity of shape memory polymers *ACS Appl. Mater. Inter.***9** 3169–75

[6] Cho J W, Kim J W, Jung Y C and Goo N S 2005 Electroactive shape-memory polyurethane composites incorporating carbon nanotubes *Macromol. Rapid Commun.* **26** 412–6

[7] Meng H and Li G Q 2013 A review of stimuli-responsive shape memory polymer composites *Polymer* **54** 2199–221

[8] Meng Q and Hu J 2009 A review of shape memory polymer composites and blends *Composites: Part* A **40** 1661-72

[9] Zhang Y F, Zhang N B, Hingorani H, Ding N Y, Wang D, Yuan C, Zhang B, Gu G Y and Ge Q 2019 Fast-response, stiffness-tunable soft actuator by hybrid multimaterial 3D printing *Adv. Funct. Mater.* **29** 1806698

[10] Anthamatten M, Roddecha S and Li J H 2013 Energy storage capacity of shape-memory polymers *Macromolecules* **46** 4230–34

[11] Santo L, Quadrini F, Squeo E A, Dolce F, Mascetti G, Bertolotto D, Villadei W, Ganga P L and Zolesi V 2012 Behavior of shape memory epoxy foams in microgravity: experimental results of STS-134 mission *Microgravity Sci. Technol.* **24** 287–96

[12] Ortega J M, Hartman J, Rodriguez J N and Maitland D J 2013 Virtual treatment of basilar aneurysms using shape memory polymer foam *Ann. Biomed. Eng.* **41** 725–43

[13] Delaey J, Dubruel P and Van Vlierberghe S 2020 Shape-memory polymers for biomedical applications *Adv. Funct. Mater.* **30** 1909047

[14] Lendlein A and Langer R 2002 Biodegradable, elastic shape-memory polymers for potential biomedical applications *Science* **296** 1673–6

[15] Xie T 2010 Tunable polymer multi-shape memory effect *Nature* 464 267–70

[16] Kuang X, Liu G M, Dong X and Wang D J 2016 Triple-shape memory epoxy based on Diels-Alder adduct molecular switch *Polymer* **84** 1–9

[17] Nguyen T D, Yakacki C M, Brahmbhatt P D and Chambers M L 2010 Modeling the relaxation mechanisms of amorphous shape memory polymers *Adv. Mater.* **22** 3411–23

[18] Yu K, Xie T, Leng J S, Ding Y F and Qi H J 2012 Mechanisms of multi-shape memory effects and associated energy release in shape memory polymers *Soft Matter* **8** 5687–95

[19] Nguyen T D 2013 Modeling shape-memory behavior of polymers *Polym. Rev.* **53** 130–52

[20] Li Y X, Hu J Y and Liu Z S 2017 A constitutive model of shape memory polymers based on glass transition and the concept of frozen strain release rate *Int. J. Solids Struct.* **124** 252–63

[21] Huang R, Zheng S J, Liu Z S and Ng T Y 2020 Recent advances of the constitutive models of smart materials-hydrogels and shape memory polymers *Int. J. Appl. Mech.* **12** 2050014

[22] Macedo P B and Litovitz T A 1965 On the relative roles of free volume and activation energy in the viscosity of liquids *J. Chem. Phys.***42** 245–56

[23] Gibbs J H and Adam G 1965 On the temperature dependence of cooperative relaxation properties in glass-forming liquids *J. Chem. Phys.* **43** 139–46

[24] Liu Y P, Gall K, Dunn M L, Greenberg A R and Diani J 2006 Thermomechanics of shape memory polymers: uniaxial experiments and constitutive modeling *Int. J. Plast.* **22** 279–313

[25] Fried J R 2014 *Polymer science and technology* (Upper Saddle River, NJ: Prentice Hall)

[26] Samuel C, Barrau S , Lefebvre J M, Raquez J M and Dubois P 2014 Designing multiple-shape memory polymers with miscible polymer blends: evidence and origins of a triple-shape memory effect for miscible PLLA/PMMA blends *Macromolecules* **47** 6791–803

[27] Liu H C, Li J B, Gao X X, Deng B and Huang G S 2017 Double network epoxies with simultaneous high mechanical property and shape memory performance *J. Polym. Res*. **25** 24

[28] Kim J, Jeon S Y, Hong S, An Y, Park H and Yu W R 2021 Three-dimensional constitutive model for shape-memory polymers considering temperature-rate dependent behavior *Smart Mater. Struct.* **30** 035030

[29] Treloar L R G 2005 *The physics of rubber elasticity* (Oxford, NY: Oxford University Press)

[30] Liu J Y, Gorbacheva G, Lu H B, Wang J Z and Fu Y Q 2022 Dynamic equilibria with glass transition heterogeneity and tailorable mechanics in amorphous shape memory polymers *Smart. Mater. Struct.* **31** 075022

[31] Cohen M H and Turnbull D 1959 Molecular transport in liquids and glasses *J. Chem. Phys.* **31** 1164–9

[32] Schweizer K S and Saltzman E J 2004 Theory of dynamic barriers, activated hopping, and the glass transition in polymer melts *J. Chem. Phys.* **121** 1984–2000

[33] Hodge I M 1987 Effects of annealing and prior history on enthalpy relaxation in glassy polymers. 6. Adam-Gibbs formulation of nonlinearity *Macromolecules* **20** 2897–908

[34] Liu J Y, Xing Z Y, Lu H B and Fu Y Q 2021 Interfacial confinement in semi-crystalline shape memory polymer towards sequentially dynamic relaxations *Int. J. Appl. Mech.* **13** 2150117

[35] Wunderlich B 1960 Study of the change in specific heat of monomeric and polymeric glasses during the glass transition *J. Phys. Chem.* **64** 1052–6

[36] Tobushi H, Okumura K, Hayashi S and Ito N 2001 Thermomechanical constitutive model of shape memory polymer *Mech. Mater.* **33** 545–54

[37] Morshedian J, Khonakdar H A and Rasouli S 2005 Modeling of shape memory induction and recovery in heat-shrinkable polymers *Macromol. Theor. Simul.* **14** 428–34